Journal of The Electrochemical Society, **149** (8) A1092-A1099 (2002)
0013-4651/2002/149(8)/A1092/8/$7.00 © The Electrochemical Society, Inc.

Development of Supported Bifunctional Electrocatalysts for Unitized Regenerative Fuel Cells

Guoying Chen,[a] Simon R. Bare,[b] and Thomas E. Mallouk[a,*,z]

[a]*Department of Chemistry, The Pennsylvania State University, University Park, Pennsylvania, 16802, USA*
[b]*UOP LLC, Des Plaines, Illinois 60017, USA*

Mixed metal catalysts containing Pt, Ir, Ru, Os, and Rh were synthesized on three different conductive oxide supports, Ebonex, which is a mixture of Ti_4O_7 and other phases, phase-pure microcrystalline Ti_4O_7, and $Ti_{0.9}Nb_{0.1}O_2$, a doped rutile compound. Ebonex-supported catalysts were prepared as arrays and screened combinatorially for activity and stability as bifunctional oxygen reduction/water oxidation catalysts. The highest activity and stability was found in the Pt-Ru-Ir ternary region at compositions near $Pt_4Ru_4Ir_1$. X-ray near edge absorption spectra indicated a significant electronic interaction between the catalyst and the support, and a substantial increase in catalyst utilization was observed, even though the support surface areas were relatively low. Both Ebonex and Ti_4O_7 have short-lived electrochemical stability under conditions of oxygen evolution at +1.6 V *vs.* RHE in 0.5 M H_2SO_4. Current at these supported catalysts gradually decreases, and the decrease is attributed to loss of electronic conductivity. Ebonex and Ti_4O_7 are also thermally oxidized in air at temperatures above 400°C. In contrast, $Ti_{0.9}Nb_{0.1}O_2$, which has a nondefective oxygen lattice, is quite resistant to electrochemical and thermal oxidation. Conditioning of $Ti_{0.9}Nb_{0.1}O_2$-supported $Pt_4Ru_4Ir_1$ at positive potentials had little effect on the activity of the catalyst.
 [DOI: 10.1149/1.1491237]

Manuscript submitted November 19, 2001; revised manuscript received February 18, 2002. Available electronically July 2, 2002.

Unitized regenerative fuel cells (URFCs) are promising energy storage systems for uninterrupted power supplies, solar-powered aircraft, satellites and micro-spacecraft, and certain terrestrial vehicles. They are also potentially useful for load leveling of distributed power generation from sources such as wind turbines and solar cells. URFCs provide very high energy density, *i.e.*, high energy storage at minimal weight, by combining an electrolyzer (in which water is converted into hydrogen and oxygen by the primary energy source) and a fuel cell (in which the recombination of the stored hydrogen and oxygen generates water and electrical energy) in the same dual mode system.[1] Although URFCs are an appealing technology for meeting these energy needs, their development is still at an early stage. One key issue is the development of corrosion-resistant and highly active electrocatalysts for both oxygen reduction and water oxidation at the oxygen electrode. Combinatorial methods are especially useful in this case, because they allow screening of catalysts that are simultaneously optimized for activity and stability in both reactions. We recently reported a combinatorial study of mixed metal and alloy catalysts for these reactions,[2] and a ternary $Pt_{4.5}Ru_4Ir_{0.5}$ catalyst was identified as an efficient and stable catalyst for the oxygen electrode in URFCs.

The importance of the support in catalysis is well recognized. Typically, the support provides a physical surface for dispersion of small metal particles, which is necessary for achieving high surface area. For electrochemical reactions, additional roles of the support are to control wettability and to provide good electronic conductivity. Carbon has generally been used in fuel cell systems, acting as an innocent conductive support with slight interactions between the supported metal particles and surface functional groups.[3,4] The use of carbon supports allows one to decrease noble metal loadings from *ca.* 4 to 0.1-0.2 mg/cm^2 in H_2/O_2 fuel cell/membrane electrode assemblies (MEA).[5,6] However, the kinetically slow, yet thermodynamically favorable electrochemical oxidation of carbon at fuel cell cathode potentials sets a practical limit on the lifetime of the supported catalyst (Eq. 1)[7]

$$C + 2H_2O \rightarrow CO_2 + 4H^+ + 4e^- \qquad E_0 = 0.118\ \text{V}\ \textit{vs.}\ \text{RHE at } 25°\text{C} \qquad [1]$$

In URFCs, high potentials at the oxygen electrode during electrolysis lead to heavy corrosion of carbon. Some work has been reported on the use of electronically conducting carbon substitutes, including boron carbide, tantalum boride, titanium carbide, and some perovskite compounds, in fuel cell systems.[8-10] Conductive oxide supports, particularly reduced titanium oxides and titanium-ruthenium oxide composites have been used in electrolyzers and are important candidates for use in the oxygen electrodes of URFCs.

Ebonex (Atraverda Ltd., U.K.) is an electrically conductive ceramic consisting of several suboxides of titanium dioxide, mainly Ti_4O_7 and Ti_5O_9, which are the most conductive compounds in a homologous series of crystallographic shear structures of the general formula Ti_nO_{2n-1} ($4 \leq n \leq 10$), collectively known as Magneli phases.[11] In spite of the presence of reduced titanium, Ebonex is electrochemically stable in both acidic and basic solutions. It also has a unique combination of high conductivity ($\sigma \approx 10^3\ \Omega^{-1}\ \text{cm}^{-1}$) and good corrosion resistance.[12] Ebonex has been widely used in ceramic electrodes in aggressive environments,[13] as a conductive matrix in microelectrode arrays,[14,15] and as a substrate for electrode materials.[12,14-20] Langer *et al.* compared Ebonex and graphite as supports for platinum and nickel electrocatalysts in the study of electrogenerative oxidation of aliphatic and aromatic alcohols.[21] In this work, an Ebonex-supported electrocatalyst array was synthesized and screened for corrosion resistance and catalytic activity in both oxygen reduction and water oxidation by fluorescence-based combinatorial screening. Optimized compositions were then prepared in bulk, tested in a gas diffusion half-cell, and characterized physically and electrochemically.

It is well known that the electronic conductivity of titanium-based ceramics originates from the presence of Ti^{3+} ions.[22] There are two ways to create Ti^{3+} ions in the rutile structure, by creating oxygen vacancies and shear planes (usually by heating TiO_2 in a reducing atmosphere) or by introducing appropriate donor dopants (*e.g.*, Nb or F). Although ceramics prepared by the reduction method are widely used as electrode materials, since Hayfield's discovery of their monolithic block form in 1978,[23] the rutile-doped ceramics have rarely been studied as electrochemical materials. Here we report the synthesis of two conductive titanium ceramics, Ti_4O_7 and $Ti_{0.9}Nb_{0.1}O_2$, made, respectively, by reducing and doping rutile titanium dioxide. We compare their activity and stability as supports for Pt-Ru-Ir URFC electrocatalysts. We show that both Ti_4O_7 and Ebonex have limited electrochemical and thermal stability to oxidation, whereas the stability of $Ti_{0.9}Nb_{0.1}O_2$ is substantially better.

* Electrochemical Society Active Member.
z E-mail: tom@chem.psu.edu

Experimental

Synthesis and testing.—Ebonex-supported combinatorial arrays were synthesized by pipetting aqueous suspensions of Ebonex onto a Teflon-coated Toray carbon sheet. Aqueous solutions of five metal salts ($RhCl_3$, H_2PtCl_6, $RuCl_3$, $OsCl_3$, and $IrBr_3$) were then dispersed onto the support by a robotic plotter (Cartesian Technologies, PixSys 3200), to a total metal loading of 20 wt % on each spot. The array was reduced and washed as described in detail elsewhere.[2,24]

Conductive Ti_4O_7 particles were synthesized using a modified literature procedure.[25] Ultrafine rutile TiO_2 was purged with argon in a tube furnace.[26] Reduction under H_2 at 1050°C for 50 min gave single-phase Ti_4O_7 powder.

$Ti_{0.9}Nb_{0.1}O_2$ was synthesized by the literature method.[27] Supported high surface area catalysts were prepared by mixing the support with the appropriate metal halide salts in deionized water to reach an overall metal concentration of 40 mM. The solution was then reduced by using excess of 5% aqueous sodium borohydride solution, and the precipitate was collected by filtration, washed thoroughly with deionized water, and dried at 80°C.

Screening of the supported arrays, as well as preparation and testing of gas diffusion half-cell electrodes was carried out as described previously.[2,24]

Characterization.—X-ray powder diffraction (XRD) patterns for as-prepared catalysts were recorded on a Philips X'Pert MPD diffractometer, using monochromatized Cu Kα radiation ($\lambda = 1.5418$ Å).

The X-ray absorption near edge structure (XANES) data were collected at the National Synchrotron Light Source (NSLS) at Brookhaven National Laboratory on beamlines X18B (Pt and Ir L_3-edges and Ru K-edge) and X19A (Ti K-edge). The synchrotron was operating at 2.5 GeV and nominal 300 mA current. On X19A a Si(111) double-crystal monochromator was used, the beam was focused using Rh-coated mirrors, and a white beam slit of 1 mm was used. On X18B the data were collected using a channel-cut Si(111) and a 1 mm white beam slit. On both beamlines the beam was detuned to minimize the effect of harmonics. The Ti K-edge data were collected in fluorescence mode using a Lytle detector, while the Pt and Ir L_3-edge XANES spectra of the supported powders were collected in transmission using appropriate amounts of catalyst, and with a 30 cm I_0 chamber filled with N_2 and 30 cm I_t chamber filled with Ar. The data from the unsupported samples were collected in total electron yield mode to avoid thickness effects. The energy calibration was performed using appropriate reference foils. The data were normalized in the usual manner using WinXAS v.2.1.[28]

X-ray photoelectron spectra (XPS) were obtained with a Kratos Analytical XSAM 800 PCI spectrometer, with a Mg Kα line source. Powder samples were dusted onto double-sided carbon tape, with a spot size of 700 μm (iris open) and a take-off angle of 80° (with respect to the sample plane). The approximate sampling depth under these conditions was 25 Å. Binding energies were referenced to a graphite standard (C 1s = 284.6 eV), and apparent atomic percentages were obtained by dividing integrated peak areas by relative sensitivity factors.

Scanning electron microscopy (SEM) images were obtained at the Electron Microscope Facility at The Pennsylvania State University, using a JEOL-JSM 5400 microscope at 30 kV accelerating voltage. Brunauer-Emmett-Teller (BET) surface area measurements were performed on a Micrometitics ASAP 2010 instrument. All the samples were dried under vacuum at 60°C for 15 h prior to analysis. Standard isotherms were obtained using liquid N_2 at 77 K, and a multipoint analysis with adsorption data from $0.08 < p/p_o < 0.15$ was used for surface area calculations.

Cyclic voltammetric studies were carried out under Ar using an EG&G PARC model 363 potentiostat/galvanostat. The catalyst inks were prepared by the method of TamizhMani *et al.*[29] All potentials are reported *vs.* reversible hydrogen electrode (RHE). The working electrodes were rotated at 2000 rpm, and cycled between −0.5 and 2 V (20 mV/s) in 0.5 M H_2SO_4, after purging with argon for 1 h. Thermogravimetric analysis (TGA) data were collected on a TA 2050 instrument in a flowing air atmosphere, at a ramp rate of 5°C/min. Inductively coupled plasma (ICP) analysis of electrolyte solutions was carried out on the Leeman Labs PS3000UV inductively coupled plasma spectrophotometer.

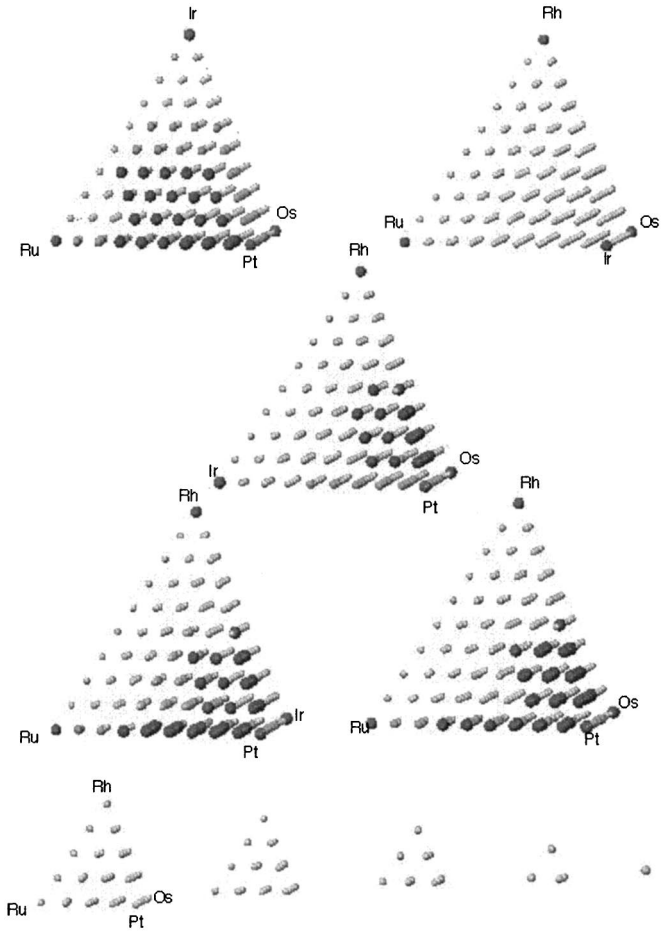

Figure 1. Supported catalyst activity map for oxygen reduction. Large tetrahedra represent quaternary regions of the map, with ternary faces, binary edges, and elemental vertices. The five smaller tetrahedra at the bottom of the figure are tetrahedral sections of the pentanary region of the composition map, with Ir content increasing progressively from left to right from 11 to 55%. Larger gray spheres indicate compositions that gave visible fluorescence from Phloxine B at +500 mV, and smaller gray spheres indicate those that were slightly less active (fluorescence at +450 mV).

Results and Discussion

Ebonex as an electrocatalyst support.—A library of 715 Ebonex-supported electrocatalysts, containing five different elements (Pt, Ru, Rh, Ir, Os) was fabricated on a Toray carbon sheet using a robotic plotter, at a total metal loading of 20% by weight. This loading level was chosen based on the common range of metal loading in supported catalysts for fuel cell systems. After sodium borohydride reduction and thorough washing with deionized water, the array was electrochemically conditioned to eliminate unstable members in the catalyst library, then screened for electrocatalytic activity for both oxygen evolution and reduction using a fluorescent detection method.[24] The screening results are expressed in three-dimensional tetrahedral sections of a four-dimensional pentanary activity map, with increments of 11% (*e.g.*, Pt_8Ir_1, Pt_7Ir_2, Pt_6Ir_3,...) along the binary edges (Fig. 1-3).[2] At this level of resolution, each

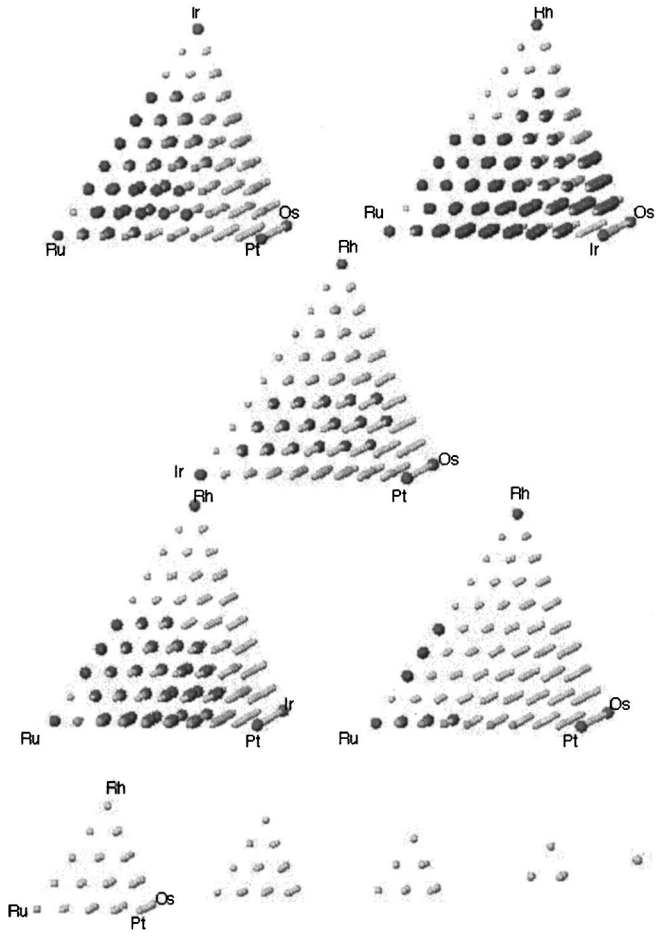

Figure 2. Supported catalyst activity map for oxygen evolution. Large and small gray spheres indicate Ni-PTP fluorescence at +1350 and +1400 mV, respectively.

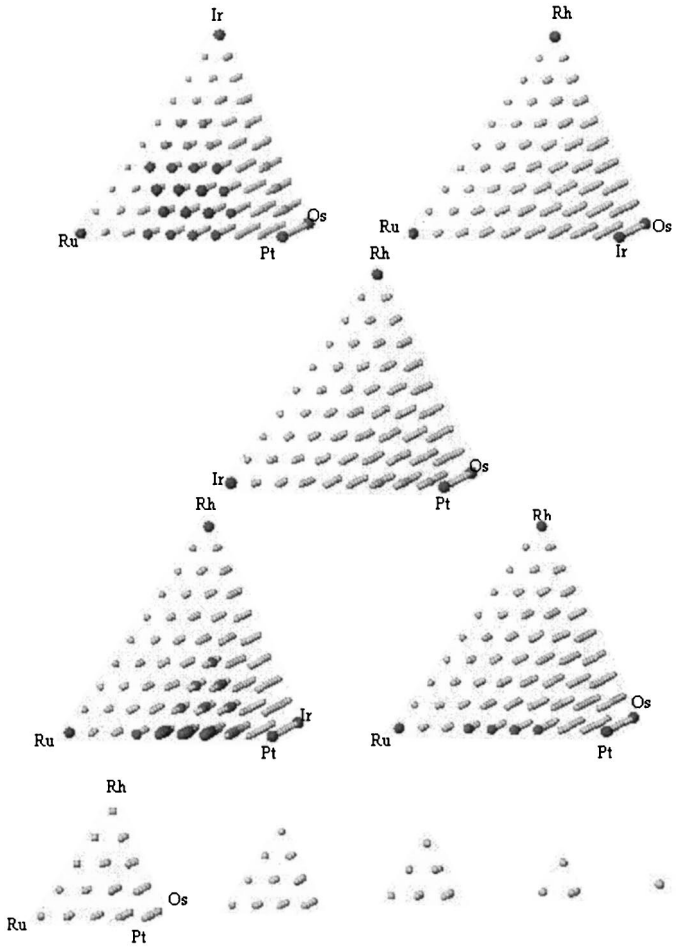

Figure 3. Consensus map for supported bifunctional catalyst activity. Larger gray spheres indicate compositions that had the highest level of activity in Fig. 1 and 2. Similar to the unsupported results, the supported Pt-Ru-Ir ternary appears on the ternary faces of two quaternary regions, *i.e.*, there is actually only one region of highest bifunctional activity. Smaller gray spheres indicate combinations of highest and next highest activity rankings from Fig. 1 and 2.

quaternary tetrahedron contains 220 unique compositions and the entire pentanary map is represented by 715 compositions. Generally, the most active supported catalysts in the library were located in the regions that were near where the best unsupported catalysts were found in our previous screening experiments.[24] Most of the hot spots for oxygen reduction were Pt rich, while those for water oxidation were Ru rich. These hot zones were broader for the supported catalysts than they were for the unsupported catalysts, primarily because the support imparts increased stability. By superimposing the activity maps, a hot-warm consensus map encompassing the most active and second most active stable catalysts for both reactions in the library was identified.

The screening experiments were carried out at relatively low resolution for the purpose of identifying high activity zones. Representative catalysts in the hot zone of the consensus map were then formulated and prepared in bulk, conditioned anodically, and then tested in a gas diffusion half-cell, in order to rank the activity of the catalysts at higher resolution. Figure 4 shows anodic (water oxidation) and cathodic (oxygen reduction) polarization curves of six Ebonex-supported ternary catalysts from the half-cell testing.

For supported Pt-Ru-Ir ternaries, the bulk testing results indicated that increasing the percentage of Pt in the catalyst improved the performance for oxygen reduction, but worsened the performance for water oxidation. This was in accord with the fluorescent screening observations. By considering the catalytic performance for both oxygen reduction and evolution, supported $Pt_4Ru_4Ir_1$ was identified as the most active catalyst in the series. Figure 5 compares the electrocatalytic activity of Ebonex-supported $Pt_4Ru_4Ir_1$ with the supported binaries, Pt_1Ru_1 and Pt_1Ir_1, supported Pt, and the unsupported $Pt_4Ru_4Ir_1$ ternary. The supported ternary catalyst displayed superior performance to all other catalysts for both oxygen reduction and water oxidation. Moreover, the amount of current generated by the Ebonex-supported $Pt_4Ru_4Ir_1$ catalyst (20 wt % metal loading) was slightly greater than the amount produced by the same weight of unsupported $Pt_4Ru_4Ir_1$ catalyst in both modes.

Generally, there are two reasons for the improvement of the catalytic activity by the inclusion of a support. First, the support acts as an inert backbone and increases the surface exposure of the catalyst and thus the utilization efficiency of the noble metals; second, the support acts as an active medium and the interaction between the metal and the support results in a change in activity through modulation of electronic structure.

Table I shows BET surface area measurement results for the Ebonex-supported catalysts. Typical surface areas of the unsupported metal catalysts were in the range of 20-30 m^2/g,[2] yet the Ebonex supported catalysts had surface areas around 10 m^2/g. Since the metal loadings in these catalysts are only 20 wt %, and the support itself has a surface area of 1 m^2/g, the higher surface area indicates that the support indeed increased metal dispersion as well as surface exposure.

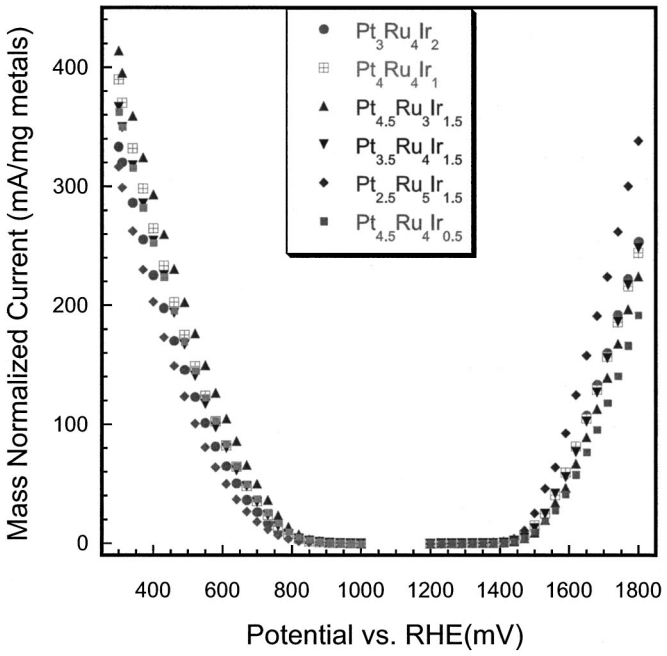

Figure 4. Polarization curves of the oxygen electrode in electrolysis (oxygen evolution) and fuel cell (oxygen reduction) modes for the indicated catalysts.

To further understand the role of the Ebonex support we collected relevant XANES data. The XANES region of an X-ray absorption spectrum (XAS), typically defined as that part of the spectrum within 50 eV of the absorption edge, primarily contains electronic information, including the oxidation state, of the element under investigation. This is typically qualitative, but often provides useful information that cannot be obtained in any other way. The XANES at the L_3-edge of an element corresponds to a transition

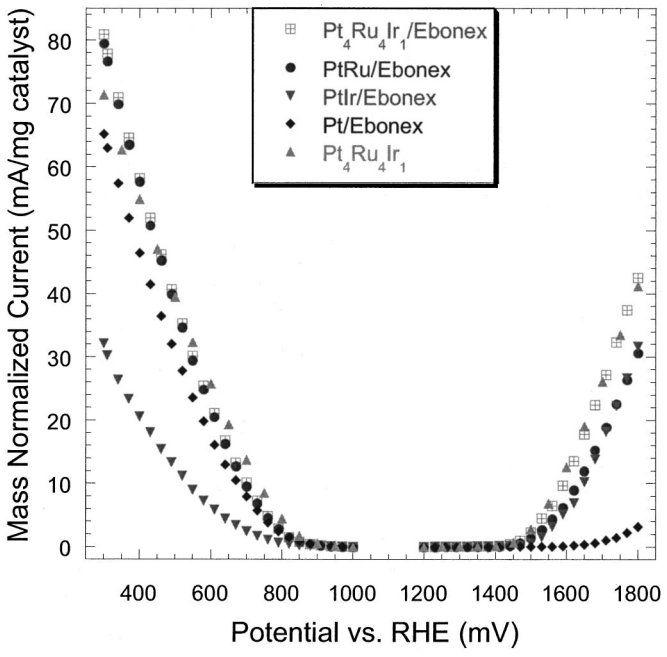

Figure 5. Polarization curves of the oxygen electrode in electrolysis (oxygen evolution) and fuel cell (oxygen reduction) modes for the indicated catalysts (Note: current is normalized to catalyst weight; catalyst = support + metal).

Table I. BET surface areas of Ebonex supported catalysts.

Catalyst composition	BET surface area (m^2/g)
$Pt_3Ru_4Ir_2$	14.1
$Pt_{4.5}Ru_3Ir_{1.5}$	12.3
$Pt_4Ru_4Ir_1$	11.2
$Pt_{4.5}Ru_4Ir_{0.5}$	8.7
Pt_1Ir_1	9.0
Pt_1Ru_1	8.7
Pt	6.7
Ebonex	1.0

from the $2p_{3/2}$ state to unoccupied *n*d states. Thus, as the number of unoccupied d states increases there is a corresponding increase in the intensity of the resonance. For example, as one moves across the third row transition metals those elements with a high density of unoccupied d density of states show a pronounced peak at the L_3-absorption edge, whereas Au with a filled d-band shows essentially a simple step function.[30] Such resonances have been widely used to probe the structure of dispersed metal catalysts.[31] For a more complete description of the unoccupied d states, use should be made of both the L_2- and L_3-edges, and indeed a quantitative determination of the fractional charge of the d band occupancy can be made by using such an approach.[32]

We begin by showing the Ti K-edge XANES of the Ebonex support and $Pt_4Ru_4Ir_1$/Ebonex (Fig. 6a). The XANES of these samples are compared to those of Ti metal and TiO_2 (anatase). The Ti K-edge XANES is sensitive both to the details of the local Ti coordination environment and also to the average Ti oxidation state.[33] First, there is a shift to a lower energy of the main absorption edge relative to that of TiO_2. This is consistent with the Ebonex having a large percentage of the Ti in a reduced oxidation state. Moreover, the overall spectral envelope at the Ti K-edge between the support, and the support plus metal, is essentially the same. This indicates that there is no gross change in the electronic structure of the Ebonex with addition of the metal.

Comparisons of the Pt L_3-edge and Ir L_3-edge XANES of 20 wt % $Pt_4Ru_4Ir_1$ and Pt_1Ir_1/Ebonex superimposed on the respective L_3-edges of the unsupported $Pt_4Ru_4Ir_1$ and Pt_1Ir_1 are shown in Fig. 6b and c. At both the Pt and Ir L_3-edges, the relative intensity of the white line resonance is greater for the supported catalyst than for the unsupported one. These data are consistent with the presence of an electronic metal-support interaction. Indeed, it is not unreasonable to conclude from the fact that the metal is highly dispersed on such a low surface area support that there is some type of chemical interaction between the metals and Ebonex. Although on many highly dispersed group VIII metal catalysts that have been reduced prior to data collection there is some residual reoxidation of the metal, manifesting itself in a slightly enhanced white line at the L_3-edge, XPS studies of the as-prepared catalysts (Table II) showed that Pt was present on the catalyst surface mainly as the metal (binding energy of 71.2 eV). There is no distinguishable difference between supported and unsupported catalyst surfaces in the amounts of possible trace oxides. Ir was present as a mixture of metal and metal oxides (binding energies of 60.6-60.9 and 62.6-63.2 eV) on both the supported and unsupported catalyst surfaces. Thus it appears that the surfaces of the catalysts prepared by the borohydride method are rich in Pt and/or Ir.

Figure 6d shows a comparison of the Ru K-edge XANES of the PtRu and $Pt_4Ru_4Ir_1$ supported and unsupported catalysts, together with data from Ru powder and RuO_2. Both the unsupported and supported catalysts show the presence of oxidized Ru, with the oxidized component for the supported catalysts being larger than the unsupported catalysts. The Ru binding energy in the XPS study also showed a mixed oxidation state (280.1, 281.1, and 282.5 eV). Com-

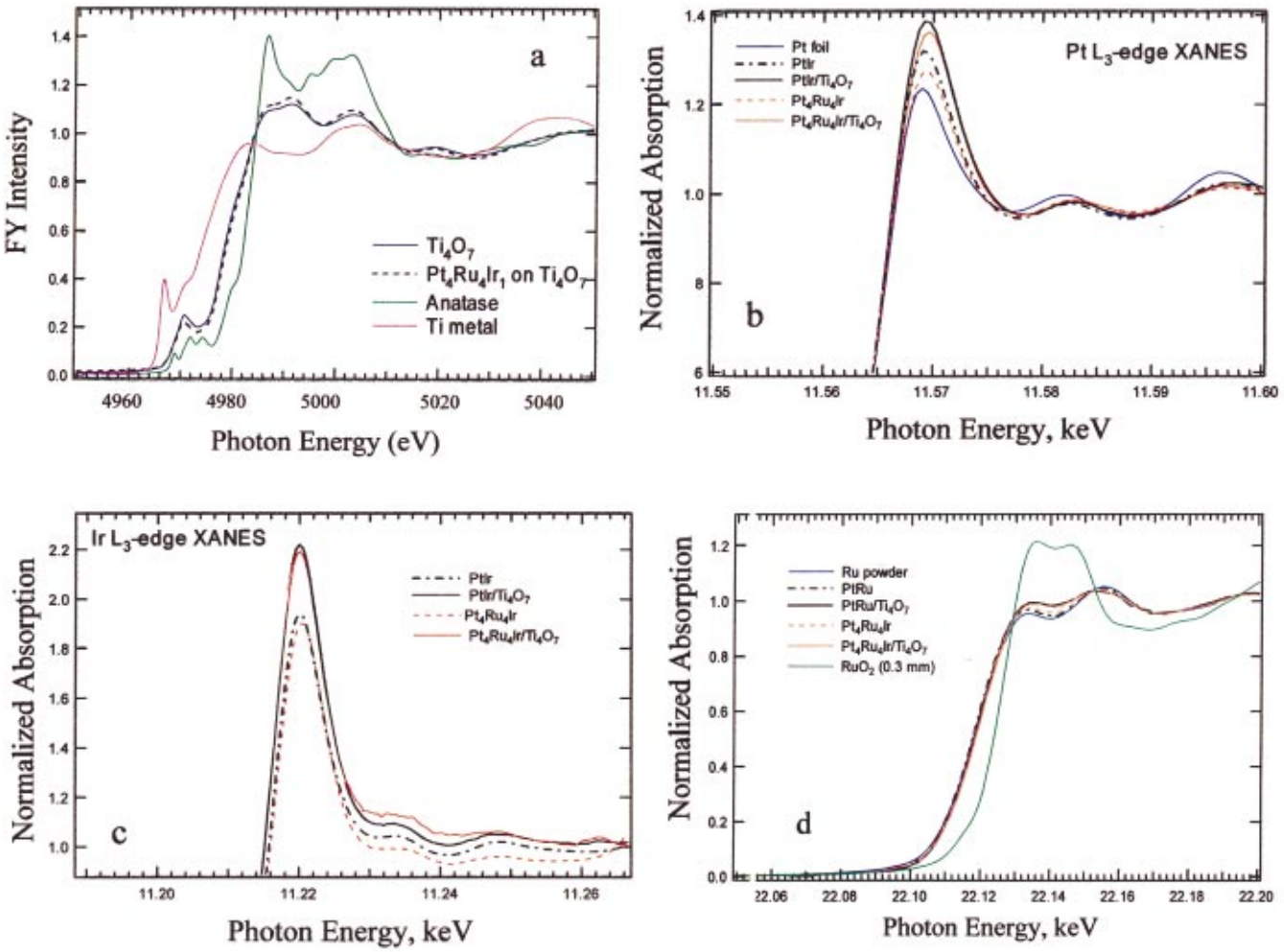

Figure 6. XANES spectra of Ebonex supported and unsupported $Pt_4Ru_4Ir_1$ and Pt_1Ir_1: (a) titanium K absorption edges, (b) platinum L_3 absorption edges, (c) iridium L_3 absorption edges, (d) ruthenium K absorption edges.

pared to the unsupported catalysts, the corresponding Ebonex-supported catalysts showed thicker RuO_x layers on the surfaces, which is consistent with the XANES results.

Powder XRD patterns showed mixed crystalline phases of the titanium suboxides, and a broad nanocrystalline face-centered cubic phase from the metal particles. The primary particle size of the metal phase was on the order of 3-4 nm, as estimated from the Scherrer linewidth equation. All of this indicates that the as-prepared catalyst is a heterogeneous mixture of metal and support.

The morphology of the Ebonex-supported catalysts was examined by SEM (Fig. 7), which showed that metal clusters were well dispersed on the support surface, and that the support has fairly large particles (in the range of 3-7 μm).

Although XPS results indicated increased amounts of metal oxides on the surface after the water oxidation and oxygen reduction reactions, there was no obvious morphological change by SEM. ICP analysis of the electrolyte also showed that very little metal was dissolved in the solution during the reactions, with less than 0.10 ppm of Pt and 2.9 ppm of Ru detected.

Figure 8 compares the catalytic activity of $Pt_4Ru_4Ir_1$/Ebonex with a commercial dimensionally stable anode (DSA, Eltech Systems Corp.) for water electrolysis. DSAs are oxide electrodes that have been widely used in industry for chlorine and oxygen evolution, and their development constitutes one of the most important advances in electrochemical technology in the last half century.[34] In

Table II. XPS data for representative Ebonex-supported catalysts.

	Apparent atomic percentages (binding energies, eV)				
Catalysts	Ti_{2p}	O_{1s}	Pt_{4f}	Ru_{3d}	Ir_{4f}
Ebonex	18.8 (458.5)	50.1 (531.0)	-	-	-
$Pt_4Ru_4Ir_1$	7.3 (459.6)	36.3 (531.0)	10.1 (71.2)	2.5 (280.1, 281.1, 282.5)	3.0 (60.9, 62.6)
PtRu	12.5 (459.0)	40.7 (531.0)	15.9 (71.2)	4.3 (280.1, 281.0, 282.4)	-
PtIr	7.8 (458.6)	46.5 (531.0)	5.7 (71.0)	-	8.1 (60.6,63.2)

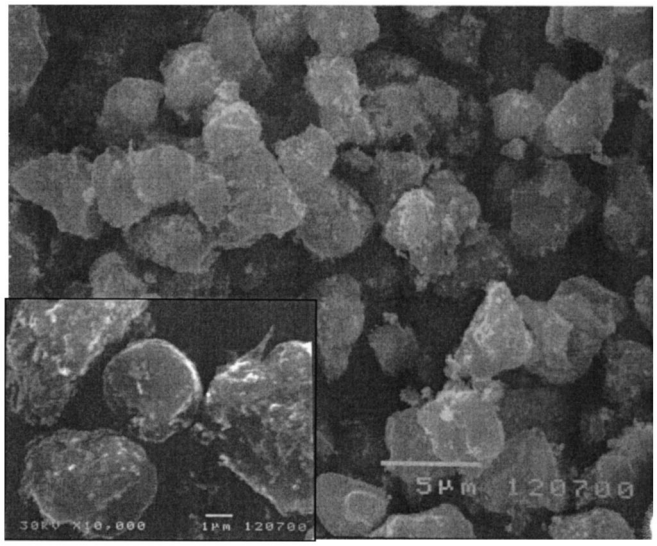

Figure 7. SEM image of Ebonex-supported $Pt_4Ru_4Ir_1$.

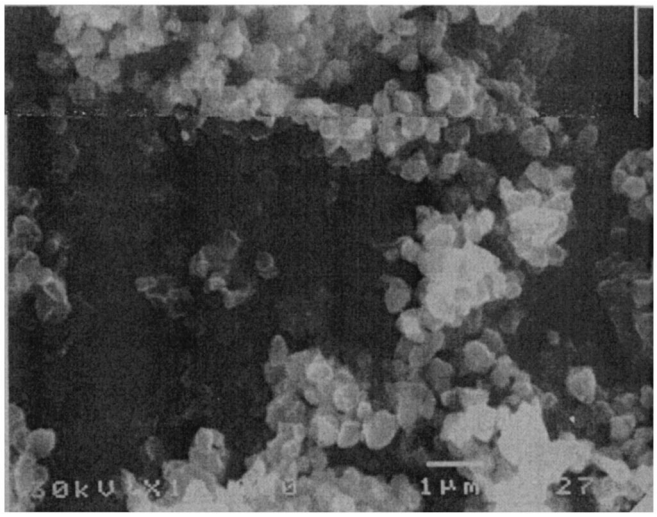

Figure 9. SEM image of Ti_4O_7 synthesized from ultrafine TiO_2.

0.5 M H_2SO_4 solution, the 20 wt % metal ternary catalyst supported on Ebonex gave slightly lower current for oxygen evolution than did the IrO_2/Ta_2O_5-coated DSA. However, when the current was normalized to either the mass of noble metal or noble metal + support, the performance of the supported ternary catalyst was better. The supported ternary catalyst was also a good catalyst for oxygen reduction, whereas the DSA was a relatively poor catalyst. Our conclusion from this comparison is that the ternary catalyst/Ebonex system has superior performance overall for regenerative fuel cells, although the mass loading and catalyst utilization still need to be optimized.

Other conductive titanium compounds as electrocatalyst supports.—To further study and optimize the supported catalyst system, we synthesized the major conductive component in Ebonex, Ti_4O_7, as a pure phase and a niobium-doped titanium dioxide, $Ti_{0.9}Nb_{0.1}O_2$, and compared their performance as electrocatalyst supports with that of Ebonex. Group 5 doping of titanium dioxide generates Ti^{III}, the conductive species in titanium compounds, without introducing defects in the oxygen lattice. The complete composition range in the system $Ti_{1-x}Nb_xO_2$ between $x = 0$ and $x = 1$ has been prepared, and the conductivity of the solid has been found to increase with the Nb-doping level over a certain range.[27,35] In this study, 10% Nb doping was chosen since this composition has been relatively well studied structurally and electronically.[36]

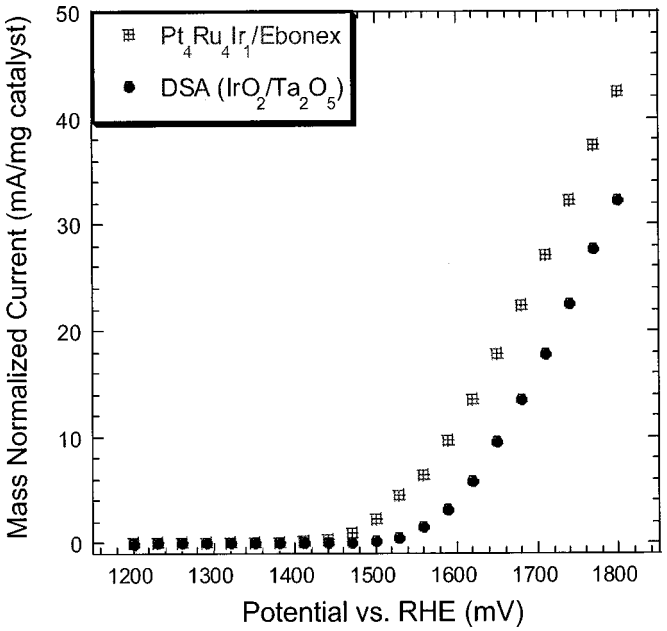

Figure 8. Polarization curves of the oxygen electrode in electrolysis mode for $Pt_4Ru_4Ir_1$/Ebonex and a commercial DSA for oxygen evolution. Currents are normalized to the mass of Ebonex + metals (for $Pt_4Ru_4Ir_1$/Ebonex) or iridium-tantalum mixed oxides (for the DSA).

The synthesis of both Ti_4O_7 and $Ti_{0.9}Nb_{0.1}O_2$ started from the same precursor, ultrafine rutile TiO_2, which was prepared by a modification of the procedure of Harada *et al.*[26] and had a BET surface area of 110 m^2/g. Ti_4O_7 was obtained by hydrogen reduction of TiO_2 at 1050°C, while $Ti_{0.9}Nb_{0.1}O_2$ was prepared by heating an intimately ground mixture of TiO_2 and NbO_2 in a sealed quartz tube under vacuum at 650°C for 1 day, 950°C for 2 days, and then 1000°C for 5 days. Both ceramic samples were dark blue in color, and had an electrical conductivity similar to Ebonex (in the range of 0.2-1.5 Ω^{-1} cm^{-1}), when measured as a pressed powder sample using a simple homemade two-point measurement device.

The XRD pattern for the Ti_4O_7 sample was in good agreement with the unit cell dimensions reported for a Ti_4O_7 single crystal by LePage and Marezie,[37] and the XRD pattern for $Ti_{0.9}Nb_{0.1}O_2$ showed a pure rutile microcrystalline phase.

Figure 9 shows an SEM image of the synthesized Ti_4O_7. Although the average diameter of Ti_4O_7 particles was estimated to be about 300-500 nm, it was also evident that there was particle aggregation and sintering in this ceramic material, due to the high temperature of the hydrogen reduction. BET surface area measurements gave relatively low surface areas for all three supports, 2 and 1.4 m^2/g for the synthesized Ti_4O_7 and $Ti_{0.9}Nb_{0.1}O_2$, respectively, and 1 m^2/g for Ebonex.

Cyclic voltammograms (CVs) of $Ti_{0.9}Nb_{0.1}O_2$ and Ebonex in 0.5 M H_2SO_4 are shown in Fig. 10. The CVs of the ceramics showed a wide potential window of stability (ranging from −0.4 to 2 V *vs.* RHE), while Vulcan XC-72R carbon, a commonly used electrocatalyst support, gave a noticeable oxidation current at positive potentials as low as 1.0 V. Interestingly, the $Ti_{0.9}Nb_{0.1}O_2$ appears to have lower anodic current at the positive potential limit of this experiment, indicating a lower background current for uncatalyzed oxygen evolution and/or a lower corrosion rate at this potential. Both supports showed minimal catalytic activity for both water oxidation and

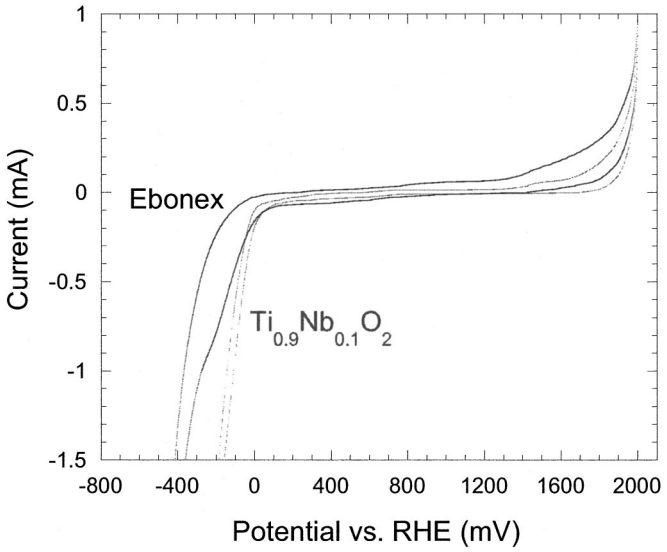

Figure 10. Cyclic voltammograms of Ebonex and $Ti_{0.9}Nb_{0.1}O_2$ recorded at 20 mV/s in a 0.5 M H_2SO_4 electrolyte solution.

oxygen reduction in acid electrolytes in the potential range studied, 0 to 1800 mV.

The best composition identified from the screening results of the Ebonex-supported array, $Pt_4Ru_4Ir_1$, was prepared in supported forms by reducing the corresponding metal salts onto synthesized Ti_4O_7 and $Ti_{0.9}Nb_{0.1}O_2$, using the borohydride method. These supported catalysts were then tested in the gas diffusion half-cell for both oxygen reduction and evolution. The Ti_4O_7-supported catalyst showed catalytic activity very similar to that of the Ebonex-supported catalyst in both reactions, while the catalyst supported on the $Ti_{0.9}Nb_{0.1}O_2$ gave higher currents at all applied voltages. Because the difference increased as the catalysts were progressively oxidized (see below), we tentatively attribute the lower current at a given bias to a greater internal IR drop in the Ebonex- and Ti_4O_7-supported catalysts.

The increased stability of $Ti_{0.9}Nb_{0.1}O_2$ is underscored by a comparison of its thermal behavior in an oxidizing atmosphere with that of oxygen-deficient materials prepared by the reduction method. Figure 11 shows TGA data for these materials under flowing air. Both Ebonex and Ti_4O_7 are oxidized to TiO_2, beginning at about 400°C and continuing to 600°C, whereas $Ti_{0.9}Nb_{0.1}O_2$ does not show a significant weight gain through 1000°C. After heating in air for 20 h at 500°C, Ebonex and Ti_4O_7 turn white and their conductivity decreases by at least five orders of magnitude, consistent with complete oxidation to a Ti(IV) oxide. Under the same conditions, the conductivity of $Ti_{0.9}Nb_{0.1}O_2$ decreases to approximately 1/1000 of its initial value and its color changes gradually from deep blue to blue-gray. This slow loss of conductivity is pertinent to the synthesis of supported catalysts, since some preparation methods (*e.g.*, molten salt methods) require high temperatures and oxidizing environments.

To further investigate their electrochemical stability, we examined Ebonex- and $Ti_{0.9}Nb_{0.1}O_2$-supported catalysts during a relatively long period of anodic polarization in the gas diffusion half-cell, with continuous 0.5 M H_2SO_4 electrolyte flow. Figure 12 shows polarization curves for oxygen reduction and water oxidation by $Pt_4Ru_4Ir_1$ supported on Ebonex and $Ti_{0.9}Nb_{0.1}O_2$, before and after a 7 h period of oxygen evolution at 1600 mV *vs.* RHE. The $Ti_{0.9}Nb_{0.1}O_2$-supported catalyst showed no significant difference in current after the polarization period. However, there is a distinct current drop for the Ebonex-supported catalyst, especially for the oxygen reduction reaction. The likely cause of this effect is partial oxidation of Ebonex, which creates a resistive layer through which

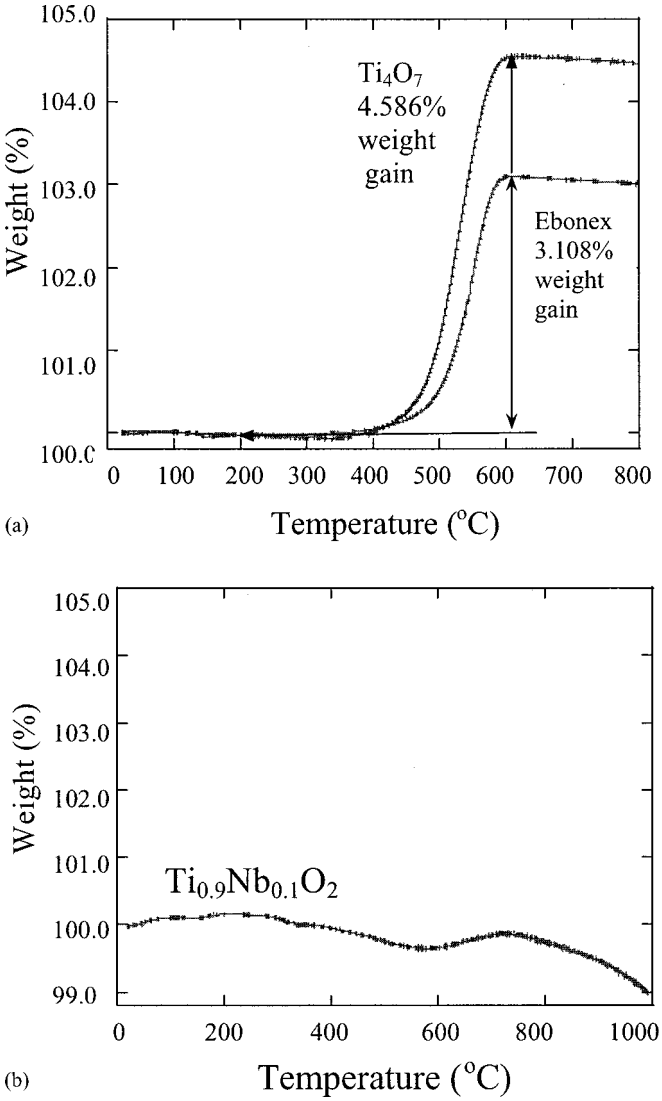

Figure 11. TGA data for the supports under flowing air (a) Ebonex and synthesized Ti_4O_7, (b) $Ti_{0.9}Nb_{0.1}O_2$.

current must pass. The loss in current shows that although they are stable for short periods of time, Ebonex and Ti_4O_7 are still oxidized to nonconductive TiO_2 at the catalyst/support/electrolyte three-phase interface after extensive polarization at the positive potentials of the oxygen electrode. On the other hand, $Ti_{0.9}Nb_{0.1}O_2$ shows good stability under these conditions.

Conclusions

Reduced titanium oxides present a viable alternative to carbon and other easily oxidized supports for use in electrolyzers and URFCs. These supports are made conductive by introducing Ti(III) into the lattice. This can be done either by reduction in a hydrogen atmosphere, or by substituting Nb for Ti. In the latter case, there is little or no anion deficiency in the structure, and so the product is significantly more stable to thermal or electrochemical oxidation. These supports substantially enhance the utilization of Pt-Ru-Ir electrocatalysts for oxygen reduction and water oxidation.

Combinatorial optimization of these supported catalysts allows one to select compositions that have high activity for both the water oxidation and oxygen reduction reactions as well as high stability. In general, the compositions that were most active as unsupported catalysts were also active with the titanium oxide supports. However, broader ranges of stable catalysts were found with the supported catalysts. The catalyst/support electronic interaction was confirmed

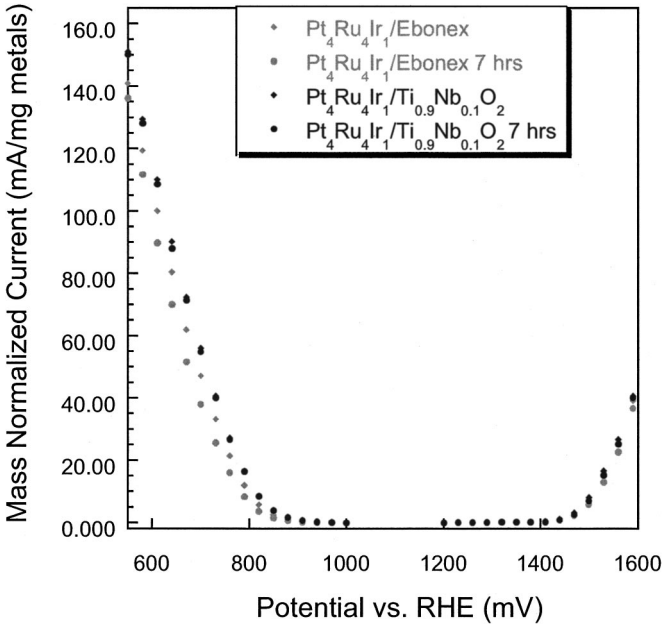

Figure 12. Polarization curves of the oxygen electrode in electrolysis and fuel cell modes for the indicated supported catalysts before and after 7 h conditioning at 1600 mV *vs.* RHE in a continuous 0.5 M H_2SO_4 electrolyte flow.

by XANES data, which showed evidence of significant metal-support electronic interaction in the supported catalysts.

Acknowledgments

This work was supported by grants from the Army Research Office (grant DAAH04-94-G-0055) and by the Army Research Laboratory, Collaborative Technology Alliance in Power and Energy. We thank Eltech Systems Corporation for supplying the DSA and Atraverda Ltd. for supplying Ebonex. Ebonex is a registered trademark of Atraverda Ltd. We thank Dr. Rosemary Walsh and the Electron Microscope Facility for the Life Sciences in the Biotechnology Institute at The Pennsylvania State University for the use of the scanning electron microscope and Dr. Jeffrey Shallenberger of The Penn State Materials Characterization Laboratory for obtaining XPS spectra. XANES studies were carried out at the National Synchrotron Light Source, Brookhaven National Laboratory, which is supported by the U.S. Department of Energy, Division of Materials Sciences and Division of Chemical Sciences.

The Pennsylvania State University assisted in meeting the publication costs of this article.

References

1. F. Mitlitsky, B. Myers, and A. H. Weisberg, *Energy Fuels*, **12**, 56 (1998).
2. G. Chen, D. A. Delafuente, S. Sarangapani, and T. E. Mallouk, *Catal. Today*, **67**, 341 (2001).
3. L. J. Hillenbrand and J. W. Lacksonen, *J. Electrochem. Soc.*, **112**, 249 (1965).
4. P. L. Antonucci, V. Alderucci, N. Giordano, D. L. Cocke, and H. Kim, *J. Appl. Electrochem.*, **24**, 58 (1994).
5. M. S. Wilson, J. A. Valerio, and S. Gottesfeld, *Electrochim. Acta*, **40**, 355 (1995).
6. G. S. Kumar, M. Raja, and S. Parthasrathy, *Electrochim. Acta*, **40**, 285 (1995).
7. G. A. Gruver, *J. Electrochem. Soc.*, **125**, 1719 (1978).
8. L. W. Niedroch and D. W. Mckee, in *Proceedings of the 21st Annual Power Sources Conference*, Atlantic City, NJ, May 16-18, 1967, PSL Publications Committee, Red Bank, NJ (1967).
9. W. T. Grubb and D. W. Mckee, *Nature (London)*, **210**, 192 (1966).
10. A. C. C. Tseung and H. L. Bevan, *J. Electroanal. Chem.*, **45**, 429 (1973).
11. S. Anderson, B. Collen, U. Kuylenstierna, and A. Magneli, *Acta Chem. Scand.*, **11**, 1641 (1957).
12. E. E. Farndon and D. Pletcher, *Electrochim. Acta*, **42**, 1281 (1997).
13. J. R. Smith, F. C. Walsh, and R. L. Clarke, *J. Appl. Electrochem.*, **28**, 1021 (1998).
14. L. He, H. F. Franzen, J. E. Vitt, and D. C. Johnson, *J. Electrochem. Soc.*, **141**, 1014 (1994).
15. L. He, H. F. Franzen, and D. C. Johnson, *J. Appl. Electrochem.*, **26**, 785 (1996).
16. S. Y. Park, S. I. Mho, E. O. Chi, Y. U. Kwon, and H. L. Park, *Thin Solid Films*, **258**, 5 (1995).
17. E. E. Farndon and D. Pletcher, *Electrochim. Acta*, **42**, 1281 (1997).
18. J. E. Graves, D. Pletcher, R. L. Clarke, and F. C. Walsh, *J. Appl. Electrochem.*, **21**, 848 (1991).
19. R. R. Miller-Folk, R. E. Noftle, and D. Pletcher, *J. Electroanal. Chem.*, **274**, 257 (1989).
20. A. Gomes, M. I. Da Silva Pereira, H. M. Mendonca, and F. M. A. Costa, *J. Appl. Electrochem.*, **25**, 1045 (1995).
21. G. R. Dieckmann and S. H. Langer, *Electrochim. Acta*, **44**, 437 (1998).
22. R. F. Bartholomew and D. R. Frankl, *Phys. Rev.*, **187**, 828 (1969).
23. P.C.S. Hayfield, U.S. Pat. 4,422,917 (1983).
24. E. Reddington, A. Sapienza, B. Gurau, R. Viswanathan, S. Sarangapani, E. S. Smotkin, and T. E. Mallouk, *Science*, **280**, 1735 (1998).
25. K. Kolbrecka and J. Przyluski, *Electrochim. Acta*, **39**, 1591 (1994).
26. H. Harada and T. Ueda, *Chem. Phys. Lett.*, **106**, 229 (1984).
27. D. Morris, Y. Dou, J. Rebane, C. E. J. Mitchell, and R. G. Egdell, *Phys. Rev. B*, **61**, 13445 (2000).
28. T. Ressler, *J. Synchrotron Radiat.*, **5**, 118 (1998).
29. G. TamizhMani, J. P. Dodelet, D. Guay, and L. Dignard-Bailey, *J. Electroanal. Chem.*, **444**, 121 (1998).
30. F. W. Lytle, P. S. P. Wei, R. B. Greegor, G. H. Via, and J. H. Sinfelt, *J. Chem. Phys.*, **76**, 1451 (1982).
31. *X-Ray Absorption Fine Structure for Catalysts and Surfaces*, Y. Iwasawa, Editor, World Scientific, Singapore (1996).
32. A. N. Mansour, J. W. Cook, and D. E. Sayers, *J. Phys. Chem.*, **88**, 2230 (1984).
33. G. A. Waychunas, *Am. Mineral.*, **72**, 89 (1987).
34. S. Trasatti, *Electrochim. Acta*, **45**, 2377 (2000).
35. (a) K. Sakata, *J. Phys. Soc. Jpn.*, **26**, 1067 (1969); (b) K. Sakata, I. Nishida, M. Matsushima, and T. Sakata, *J. Phys. Soc. Jpn.*, **27**, 506 (1969).
36. (a) Y. Gao, Y. Liang, and S. A. Chambers, *Surf. Sci.*, **365**, 638 (1996); (b) Y. Gao, *Thin Solid Films*, **346**, 73 (1999).
37. Y. LePage and M. Marezie, *J. Solid State Chem.*, **53**, 13 (1984).